


I.Z. KOZMA   
G. ALMÁSI  
J. HEBLING

# Geometrical optical modeling of femtosecond setups having angular dispersion

Department of Experimental Physics, University of Pécs, Ifjúság 6, 7624 Pécs, Hungary

Received: 29 July 2002/Revised version: 22 October 2002  
Published online: 29 January 2003 • © Springer-Verlag 2003

**ABSTRACT** A reliable and efficient method based on a geometrical optical approach is presented to model the propagation of ultrashort pulses in optical systems. It is shown that the commonly used method to determine the group delay of the spectral components of a pulse from their geometrical optical path lengths is only correct for aberration-free optical systems. In the case of systems with angular dispersion and imaging errors, a correction to the path values obtained from ray-tracing calculations must be applied, since for specific systems neglect of the correction causes significant errors. A technique for performing this correction is presented. Two optical arrangements used for the generation and detection of tunable THz radiation by the femtosecond tilted-pulse-front excitation technique are analyzed to demonstrate the indispensability of the correction.

**PACS** 42.15.-i; 42.15.Dp; 42.15.Eq; 78.47.+p

## 1 Introduction

Numerical results provided by ray-tracing algorithms of optical design programs give accurate information on the spatial properties of the imaging optical system. In the case of systems implementing measurements at high temporal resolution, the temporal deformation of the applied ultrashort optical pulses is not negligible: aside from the conventional aberrations, temporal pulse distortions should also be considered. The propagation and distortion of femtosecond pulses in optical systems can be described using wave optical theory. Several papers have discussed the temporal and spatial intensity distribution of a femtosecond laser beam [1, 2]. These simulations, based on a wave optical description of the problem, have confirmed results obtained from geometrical optics [3]. However, wave optical models are difficult to use in practice due to the complicated numerical calculations they require. Furthermore, several simplifications and approximations must be made to retain a simple model, which can be used in the assessment of practical applications. Attempts at reliably modeling femtosecond beam delivery using ray-tracing calculations are attractive for their

simplicity and speed [4, 5]. Therefore it appears worthwhile to develop methods that determine the group delay from the geometrical optical path length.

## 2 The geometrical optical approach

In a dispersive system, the phase velocity of  $v^{\text{ph}} = \omega/k$  a wave and the group velocity  $v^{\text{gr}} = \partial\omega/\partial k$  of a wave packet centered at frequency  $\omega$  are functions of frequency, where  $\omega$  is the angular frequency of the radiation and  $k$  the wave number. A short pulse propagating through this system will change its shape as it propagates. Usually, a system is designed by specifying its layout and elements, whose dispersive properties are given by the coefficients of the expansion of the spectral phase function  $\phi(\omega)$  to a Taylor series:

$$\phi(\omega) = \sum_n \frac{1}{n!} \phi^{(n)}(\omega_0) (\omega - \omega_0)^n, \quad (1)$$

where  $\phi^{(n)}(\omega_0)$  is the  $n$ th derivative of the phase function with respect to the frequency evaluated at a reference angular frequency  $\omega_0$ . The term  $\phi^{(1)}(\omega_0)$ , the so-called group delay  $\tau$ , is the time taken for a wave packet centered at the reference frequency to propagate between the reference planes. Starting from

$$\tau = \frac{d\phi(\omega)}{d\omega} \quad (2)$$

and transforming the frequency into wavelength dependence, a commonly applied formula is obtained to calculate the group delay of the pulse upon propagation through a medium with dispersion:

$$\tau = \frac{1}{c} \left( nL - L\lambda \frac{dn}{d\lambda} - n\lambda \frac{dL}{d\lambda} \right), \quad (3)$$

where  $L$  is the geometrical path length of light in a medium having a refractive index  $n$ , and  $c$  is the speed of light in a vacuum. For a specific arrangement, once the optical path  $L$  as a function of wavelength has been determined and the accumulated group delay in each optical medium the pulse is propagating through has been added up, information on the distortions of the pulse upon exiting the system can be obtained. The typical way to characterize distortions based on

ray-tracing analysis is to determine the difference in the group delays of the short- and long-wavelength components (usually the wavelengths where the spectral intensity of the pulse reaches half its maximum value). The derivatives in (3) are approximated by the difference quotients for two adjacent wavelengths  $\lambda_1$  and  $\lambda_2$ :

$$\frac{dn}{d\lambda} = \frac{n(\lambda_1) - n(\lambda_2)}{\lambda_1 - \lambda_2} \quad (4)$$

and

$$\frac{dL}{d\lambda} = \frac{L(\lambda_1) - L(\lambda_2)}{\lambda_1 - \lambda_2} \quad (5)$$

Clearly, (3) is correct only for cases when rays of different wavelengths originating from the same point on the object meet again at one point in the image plane; that is, the optical system is aberration-free. Otherwise there is a need for correction. In Sect. 5 we propose a correction method. According to our knowledge there is no reference in the literature for applying such a correction. The significance of errors caused by the neglect of corrections is specific to the geometry of the modeled arrangement. In our earlier work on the modeling of pump arrangements for the generation of laser-induced dynamic gratings [6], for example, it was obtained that the omission of correction caused an error of only 2 fs for the investigated setups, which was negligible when compared to the 25 fs assumed pulse duration. In order to demonstrate the necessity of the correction, in the following we present results of ray-tracing simulations of pulse propagation through optical setups used for the generation of tunable THz radiation by the recently reported femtosecond tilted-pulse-front excitation technique [7].

### 3 Excitation geometry for THz generation

These optical arrangements realize a novel excitation geometry that makes velocity matching possible between the exciting visible ultrashort light and THz radiation in a dielectric crystal below the phonon frequency. The important feature of the tilted-pulse-front technique is illustrated in Fig. 1: the pulse front of the light beam is tilted by angle  $\gamma$

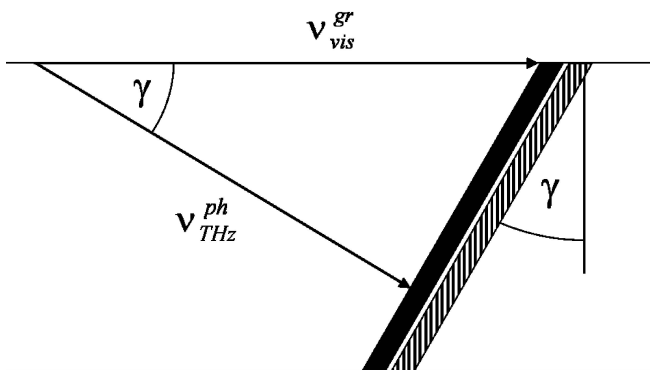


**FIGURE 1** Scheme of the impulsive phonon-polariton generation using a tilted pulse front. The ultrashort light pulse propagates to the right, while the polariton propagates perpendicularly to the generating pulse front, that is, at an angle  $\gamma$  with respect to the optical pulse

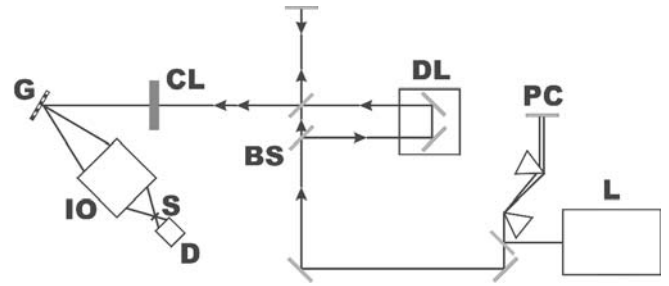


**FIGURE 2** Schematic of the experimental setup for the generation and detection of THz radiation: pre-compression is introduced by a prism compressor **PC** to the pulse from the Ti : sapphire laser, **L**. The slight tilting of the 50% beam splitter **BS** vertically separates the pump and the probe beam. The latter is sent through a rapid scan delay line, **DL**. A cylindrical lens **CL** focuses the pump and the probe pulses onto the grating **G**, which introduces the tilt of the pulse front. The grating is imaged into the sample **S** by a system of imaging optics **IO**. The transmission of the probe pulses is detected by a detector **D**

with respect to the phase front, which is perpendicular to the propagation direction of the light beam. The THz radiation (in non-linear material the phonon-polariton) excited impulsively along the pulse front propagates according to Huygens' principle perpendicularly to this front, with velocity  $v_{\text{THz}}^{\text{ph}}$ . In this case, not the velocity of the light pulse  $v_{\text{vis}}^{\text{gr}}$  [8], but its projection onto the propagation direction of the THz radiation has to be equal to  $v_{\text{THz}}^{\text{ph}}$ . Thus the velocity matching condition reads

$$v_{\text{vis}}^{\text{gr}} \times \cos \gamma = v_{\text{THz}}^{\text{ph}} \quad (6)$$

enabling effective THz generation in materials with even a significantly larger dielectric constant in the far-infrared than in the visible, just by proper choice of  $\gamma$ .

The experimental scheme capable of the generation and detection of THz radiation is shown in Fig. 2. The primary source of ultrashort pulses is a Ti:sapphire oscillator delivering 25 fs pulses at 810 nm. The presence of phonon-polaritons generated by the pump pulses is monitored by measuring the transmission of identical probe pulses with variable delay. The tilt of the pulse front of the pump and probe is introduced by diffraction off a reflection grating. The grating is imaged into the non-linear material (a 100- $\mu\text{m}$  thick GaP crystal) by different imaging optics to increase the tilt angle of the pulse front [9].

### 4 The optical arrangements analyzed

In this paper, we discuss simulations of two possible optical arrangements for imaging the grating into the sample; one consists of a spherical lens, the other is a telescopic system consisting of two confocal spherical lenses. In the second case, the grating is placed at the front focal plane of the first lens and the grating is image-relayed at the back focal plane of the second lens. Figure 3 shows detailed views of the optical path of the central and the boundary rays of the pump beam from the grating to the sample for both setups. The rays shown are at the 810 nm central wavelength and at the two edges of the assumed 30 nm spectral bandwidth (FWHM), which corresponds to a pulse width of 23 fs, assuming sech<sup>2</sup>-shaped pulses. The pump and the probe beams are superimposed upon the transmission grating at a finite angle. Their projections on the plane of the drawing are overlapping

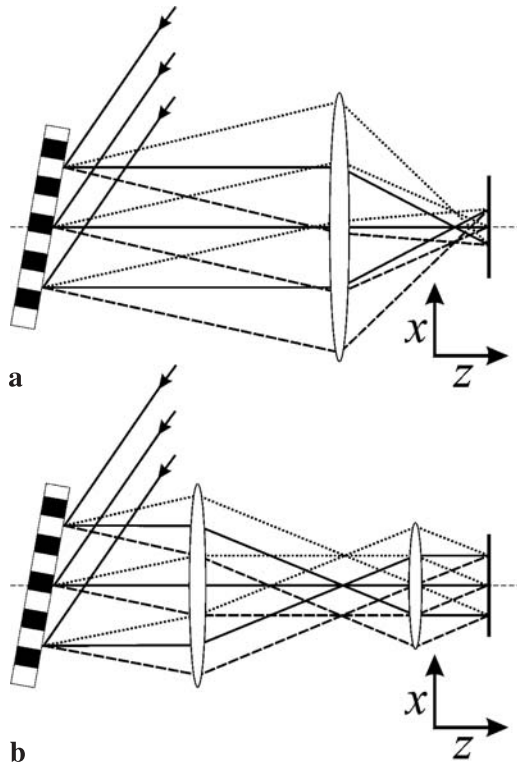


**FIGURE 3** Optical paths of central and boundary rays of the pump pulse at the central wavelength (*solid line*), and at the long- (*dotted line*) and short-wavelength edges (*dashed line*) of the bandwidth when the reflection grating is imaged by a spherical lens (**a**) and with a telescope comprised of two spherical lenses (**b**)

each other. For the sake of clarity, the plots are strongly distorted to counterbalance the difference in the scales along the optical axis  $z$  and axis  $x$ , which is perpendicular to it.

Both setups realize demagnification with the same sagittal demagnification factor of 3. Data of commercially available typical high-numerical-aperture spherical achromatic doublets are used in our models. The single lens has a focal length of 50 mm (Linco AG catalogue number: 322265). The elements of the telescope are near-IR doublets and have focal lengths of 60 mm and 20 mm (Edmund Industrial Optics catalogue numbers are NT45-798 and NT45-786), respectively.

The pulse front tilt introduced by the diffraction grating depends on the angular dispersion of the grating for a given wavelength [10, 11]:

$$\tan \gamma = \lambda \times \frac{d\beta}{d\lambda}, \quad (7)$$

where  $d\beta/d\lambda$  is the angular dispersion of the beam. To achieve the required tilt of the pulse front, a reflection grating having high grating groove density  $G = 12001/\text{mm}$  is used. In the examined cases the angular spread of the spectrum of the first diffraction order practically fills in the entire numerical aperture of the lenses. Rays of different wavelength will propagate through the lenses at different heights above the optical axis and traverse the systems along different paths. Necessarily, when using the spherical surfaces of the lenses not only in the paraxial region, monochromatic aberrations become significant as well.

## 5 The proposed method and simulation results

Due to the imaging errors, rays originating from one point on the object will miss each other on the image plane. This situation is illustrated in Fig. 4. (Again, the drawing is greatly distorted to facilitate the understanding of the problem.) Using the optical path lengths  $L_1$  and  $L_2$  of rays having wavelengths  $\lambda_1$  and  $\lambda_2$ , respectively, in (4), and then substituting the values of the obtained difference quotients into (3) to calculate the group delay, one obtains an implausible result. This is due to the fact that even a small spectral separation  $\Delta\lambda$  results in a significant spatial separation of the rays, and the optical path lengths no longer correspond to the same phase front. This can be compensated for by intersecting the optical paths with a line perpendicular to the bisector of the two rays, and subtracting the distance  $s_1$  between the point of intersection  $P'_1$  and the image point  $P_1$  from  $L_1$ , and adding the distance  $s_2$  between the point of intersection  $P'_2$  and the image point  $P_2$  to  $L_2$ .

Note that in our calculations we only considered the projection of the lines and points onto the  $xz$  plane. The fact that the imaging errors of the systems are more significant in this plane than in the  $yz$  plane permits this simplification. When the omission of the correction for errors in the  $yz$  plane would cause similar inaccuracies, the compensation technique should be extended to that plane as well in a likewise fashion, making the calculations more complicated. Figure 5 shows the results of two series of calculations for both setups; in one the necessary correction is omitted and in the other it is applied to the optical path lengths. The arrival times as a function of  $x$  vertex position for the short- (solid line) and long-wavelength (dotted line) components (at the edges of the 30 nm spectral bandwidth) are depicted in Fig. 5a for the one-lens setup, and Fig. 5b for the telescopic system. The plots corresponding to the calculations without the correction are indicated in all cases by bar symbols. In both cases the tilt of the pulse front changes slightly upon applying the correction.

There is a more conspicuous difference between the temporal separation of the two spectral components obtained

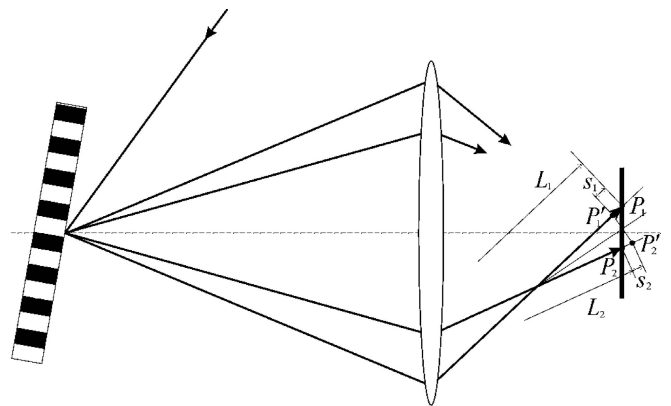


**FIGURE 4** Diagram for calculation of the group delay. The optical path lengths of rays from the grating to the image plane having a  $\Delta\lambda$  spectral separation are labeled as  $L_1$  and  $L_2$ . They should be modified by subtracting and adding the value of  $s_1$  and  $s_2$ , respectively

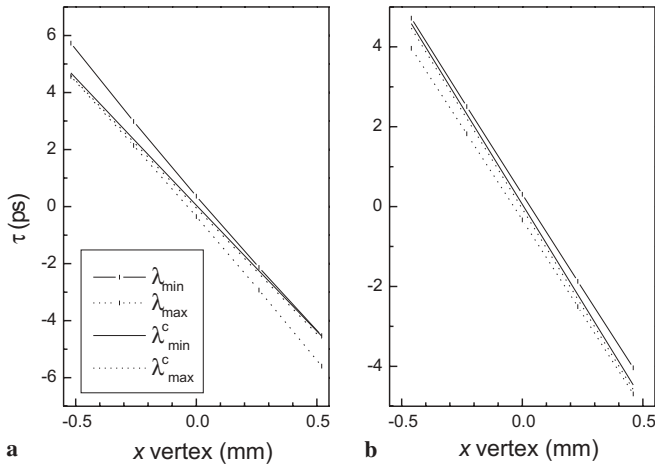


**FIGURE 5** Calculated group delay as a function of the distance from the center of the imaged area for the one-lens setup (a) and for the telescopic system (b). The bar symbols denote the uncorrected values for both the short- (solid line) and the long-wavelength (dotted line) components

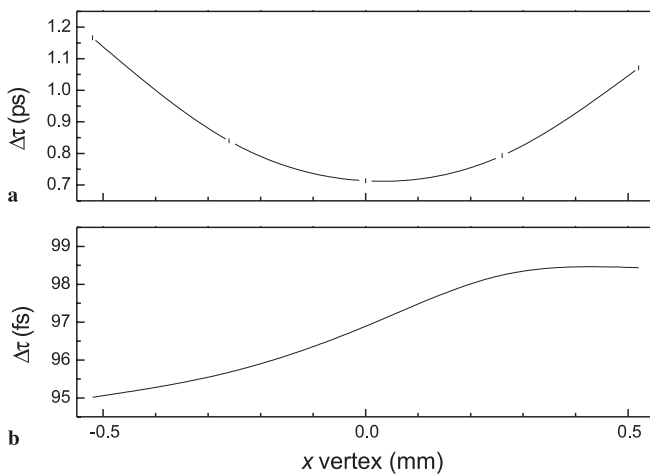


**FIGURE 6** Uncorrected (a) and corrected (b) group-delay difference for the one-lens imaging system

with the different calculation methods. Figure 6a gives the difference in the arrival times for the two extreme spectral components as a function of the distance from the center of the imaged area for the one-lens imaging system when calculating with the uncorrected optical path-length values. The obtained group delay difference is around 1 ps. This unrealistic value decreases to a value around 97 fs upon applying the corrections (see Fig. 6b). Part of this temporal dispersion arises from the lens material. We calculated for the two wavelengths examined the difference between the group delays due to material dispersion of the achromatic doublet used in the model for the one-lens setup. For the axial ray this value was 40 fs. In Fig. 7 we show the (a) uncorrected and (b) corrected group-delay difference for the telescopic system. In this case, the 680-fs value reduces to a difference of merely 113 fs between the two extreme spectral components. The group-delay difference for these wavelengths resulting from the material dispersion of the two achromatic doublets is 111 fs for the axial ray. The pulse broadening due to group delay dispersion can be eliminated by pre-compensating with a pair of prisms, since the vari-

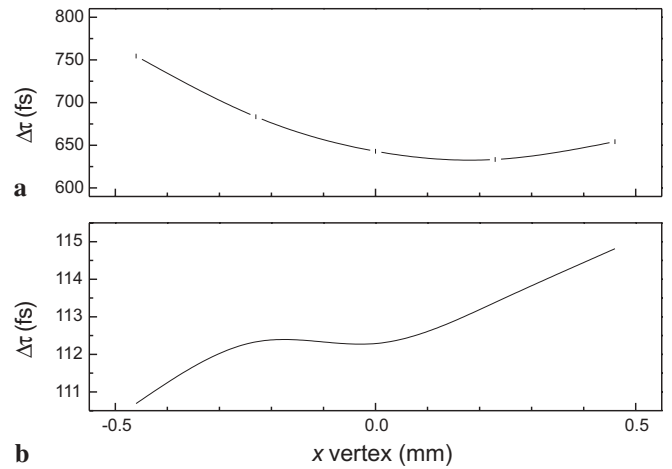


**FIGURE 7** Uncorrected (a) and corrected (b) group-delay difference for the telescopic system

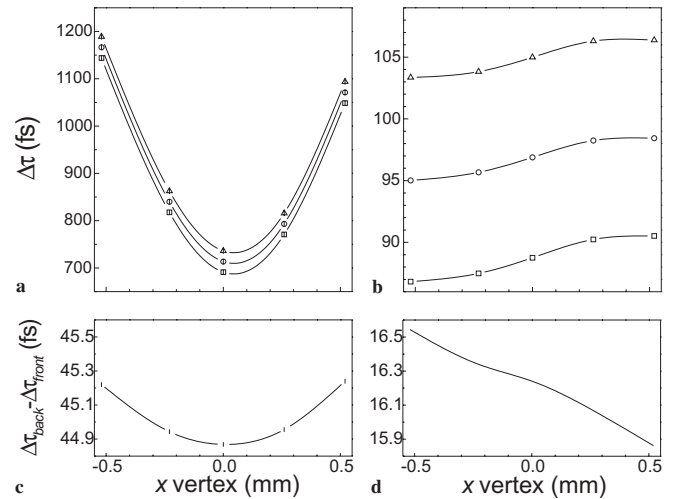


**FIGURE 8** Uncorrected (a) and corrected (b) group delay difference for the one-lens setup when the image plane is in the middle (circle), on the front (square) and on the back (triangle) surface of the 100- $\mu\text{m}$  thick sample. The corresponding uncorrected (c) and corrected (d) temporal broadening of the pulse in the sample

ation of the chirp along the pulses in both cases remains below 5 fs.

Another important aspect is the pulse propagation in the sample. We ran simulations for the one-lens setup to determine the group delay in the middle of the 100- $\mu\text{m}$  thick GaP, and 50  $\mu\text{m}$  before and 50  $\mu\text{m}$  behind this plane, that is, at the front and back surfaces of the sample. Figure 8a and b depicts the uncorrected and the corrected group-delay difference, respectively. The change in the group-delay difference between the back and the front surface of the sample yields the temporal broadening of the pulses as they propagate through the sample. These  $\Delta\tau_{\text{back}} - \Delta\tau_{\text{front}}$  values resulting from the uncorrected and corrected calculation methods are given in Fig. 8c and d, respectively. Comparing the values obtained with the 16.2-fs temporal broadening that follows from the material dispersion of GaP, it is again obvious that applying the correction to the length of the optical paths calculated by ray-tracing code gives accurate results for the modeling of short-pulse propagation.

## 6 Conclusions

The method of determining the group delay of the spectral components of a pulse from their geometrical optical path lengths has been improved. It has been shown that the commonly applied method for the modeling of ultrashort-pulse propagation in optical systems can give inaccurate results in the case of setups having angular dispersion and imaging errors. This is, to our knowledge, the first description of this limitation. A technique has been developed to overcome this problem by applying a correction to the path values obtained from ray-tracing calculations. Case studies of two optical arrangements used for the generation and detection of tunable THz radiation by the femtosecond tilted-pulse-front excitation technique were analyzed to demonstrate the indispensability of the correction. The method developed is a reliable and efficient tool for

the characterization and optimization of femtosecond optical systems.

**ACKNOWLEDGEMENTS** This work was supported by the Hungarian Scientific Research Fund under Grant No. T 038372.

## REFERENCES

- 1 Z. Bor, Z.L. Horváth: *Opt. Commun.* **94**, 249 (1992)
- 2 M. Kempe, W. Rudolph: *Opt. Lett.* **18**, 137 (1993)
- 3 Z. Bor: *J. Mod. Opt.* **35**, 1907 (1988)
- 4 J. Jiang, Z. Zhang, T. Hasama: *J. Opt. Soc. Am. B* **19**, 678 (2002)
- 5 E. Gouliemakis, G. Nersisyan, N.A. Papadogiannis, D. Charalambidis, G.D. Tsakiris, K. Witte: *Appl. Phys. B* **74**, 197 (2002)
- 6 I.Z. Kozma, J. Hebling: *Opt. Commun.* **199**, 407 (2001)
- 7 J. Hebling, G. Almási, I.Z. Kozma, J. Kuhl: *Opt. Exp.* **10**, 1161 (2002)
- 8 A. Nahata, A.S. Weling, T.F. Heinz: *Appl. Phys. Lett.* **69**, 2321 (1996)
- 9 S. Szatmári, G. Kuhnle, P. Simon: *Appl. Opt.* **29**, 5372 (1990)
- 10 Z. Bor, B. Rácz: *Opt. Commun.* **54**, 165 (1985)
- 11 J. Hebling: *Opt. Quant. Electron.* **28**, 1759 (1996)